



Trehalose-loaded LNPs enhance mRNA stability and bridge in vitro in vivo efficacy gap



Xu-Han Liu^{1,2,3,4}, Hui-Ping Song⁵, Ling-Ling Tao^{1,2,3,4}, Zhe Zhai^{1,2,3,4}, Jin-Xing Huang^{1,2,3,4} & Yong-Xian Cheng^{1,2,3,4} ✉

Lyophilization enhances mRNA vaccine stability, but conventional approaches using external trehalose for lipid nanoparticle (LNP) colloidal stability neglect mRNA chemical degradation and are compromised in vivo efficacy. Here, we report a dual-function trehalose strategy integrating its external and internal roles within LNP. This strategy enables trehalose to externally form a vitrified matrix that preserves LNP colloidal integrity, while internally stabilizing mRNA through hydrogen bonding, markedly reducing chemical degradation during storage compared to LNP relying solely on externally added trehalose. Crucially, co-loaded trehalose is co-delivered into cells, bridging the in vitro-in vivo gap by mitigating oxidative stress through reduced reactive oxygen species (ROS) and malondialdehyde (MDA) alongside elevated glutathione (GSH) and superoxide dismutase (SOD). This is corroborated by downregulated cytoplasmic and nuclear nuclear factor erythroid 2-related factor 2 (Nrf2) expression. Our strategy provides a simple, universally adaptable, and scalable method to enhance mRNA-LNP formulations stability without exogenous components or complex lyophilization steps.

Vaccines are one of the most cost-effective methods to prevent infectious diseases. mRNA vaccines are promising candidates due to their rapid development and low-cost manufacture¹. Implementing a relatively simple, independent manufacturing process significantly expedited both time and cost in the development of a new vaccine, particularly amidst a pandemic scenario marked by the emergence of severe acute respiratory syndrome coronavirus 2 (SARS-CoV-2) variants². Although mRNA vaccines hold great promise, their clinical translation and commercialization are still encountering challenges, as mRNA is highly susceptible to hydrolysis, oxidation³ and RNase enzymes⁴. The short shelf life and ultracold storage requirement of mRNA vaccines slow down their distribution mostly in resource-poor countries of the world, as maintaining ultracold storage conditions is expensive and difficult to arrange^{5,6}. Freeze-drying is a commonly used technique to improve the stability of mRNA vaccines^{7,8}. Current typical freeze-drying methods relying on simply mixing lyoprotectants (e.g., trehalose or sucrose) outside the formulation^{9,10} and optimizing the lyophilization process, including parameters such as cycle times, temperature, vacuum levels, and buffer conditions. While these factors are critical, they

are costly and require precise control, often necessitating expensive equipment and complex operations, which lead to significant batch-to-batch variations and increased production costs. Moreover, these methods mainly focus on maintaining the colloidal stability of mRNA-loaded lipid nanoparticles (LNPs)¹¹. Nevertheless, while some formulations retain structural integrity and encapsulation efficiency (EE) after lyophilization, their in vivo transfection efficiency remains reduced for unknown reasons^{8,10,12}. Therefore, it is essential to develop new strategies to enhance the stability of lyophilized mRNA vaccines, bridge the in vitro-in vivo stability gap, and reduce the risks and costs associated with inaccurate efficacy evaluations during storage.

The stability or the efficacy of lyophilized mRNA vaccines is mainly determined by: (1) the colloidal stability of the delivery system (e.g., LNPs) (2) the chemical stability of the mRNA molecular, and (3) the effect of lyoprotectants on the targeted cells being transfected. Firstly, lyoprotectants can form a stable glassy state, which immobilizes the formulation within a rigid, amorphous, glassy sugar matrix during freeze-drying. This “vitrification theory” effect significantly decreases the formation of ice crystals and

¹Guangdong Provincial Key Laboratory of Chinese Medicine Ingredients and Gut Microbiomics, Shenzhen University, Shenzhen, China. ²Institute for Inheritance-Based Innovation of Chinese Medicine, Shenzhen University, Shenzhen, China. ³Marshall Laboratory of Biomedical Engineering, Shenzhen University, Shenzhen, China. ⁴School of Pharmacy, Shenzhen University Medical School, Shenzhen University, Shenzhen, China. ⁵Department of Traditional Chinese Medicine, Qingdao Central Hospital, University of Health and Rehabilitation Sciences, Qingdao, China.

✉ e-mail: yxcheng@szu.edu.cn

prevent their mechanical damage to the colloidal stability of the delivery system¹³. Secondly, lyoprotectants form hydrogen bonds with the mRNA, effectively replacing hydrogen bonds that would otherwise form between water and the mRNA during lyophilization. This “hydrogen bonds replacement” helps maintain the native conformation and the chemical stability of mRNA^{9,14}. On the other hand, some lyoprotectants also possess anti-oxidant properties, offering additional protection to the transfected cells, which are vulnerable to oxidative stress induced by the cationic LNPs^{15,16}. For example, trehalose, which accumulates notably during heat shock and stationary phase across various organisms, can enhance thermotolerance, reduce denatured protein aggregation, and protect cells from oxygen radicals^{17–19}. Although lyoprotectants can protect mRNA vaccines through various mechanisms, current external incorporation methods can only maintain the vaccine’s colloidal stability¹³. The chemical stability of mRNA molecules is often overlooked. Additionally, the immunological effect of lyoprotectants has received little attention, even though they are co-administered with the rehydrated vaccine in humans^{10,20}. It has been reported that trehalose can enhance transfection efficiency when co-existed with transfection reagents¹⁶. However, the current lyophilization strategy, which places the lyoprotectant like trehalose externally in LNPs, faces the issue of trehalose being inefficiently co-delivered with the LNPs to target cells in vivo. This may be the reason for the discrepancy between the in vitro and in vivo performance of mRNA efficacy.

To enhance the freeze-drying stability of mRNA-LNP formulations and bridge the gap between the in vitro and in vivo performance, we proposed a dual-function trehalose loading strategy. In this method, trehalose

functions not only as an external lyoprotectant but also as a component that is co-loaded with mRNA within LNPs. During freeze-drying, external trehalose protects the colloidal stability of the LNPs, while internal trehalose replaces water and interacts with mRNA via hydrogen bonding, enhancing the chemical stability of mRNA by restricting its molecular mobility. Furthermore, internal trehalose can enter target cells along with LNPs during in vivo evaluation, providing additional protection to transfected cells vulnerable to oxidative stress induced by LNPs and enhancing in vivo transfection efficiency (Fig. 1). With this dual-function strategy, both the chemical stability of the mRNA and the immunological effects of trehalose on targeted cells could be well addressed. Herein, the preparation and characterization of trehalose-loaded LNPs were systematically analyzed. Both the in vitro and in vivo transfection efficiencies of these formulations after storage for various time periods were evaluated. After freeze-drying and storage, the colloidal stability of the formulation and the chemical stability of mRNA were also analyzed.

Results and Discussion

Briefly, the trehalose-loaded LNP (TL-LNP) was prepared using a nanoprecipitation and solvent evaporation method as illustrated in Fig. 2A. The freshly prepared LNP without trehalose exhibited a size distribution by intensity measurements of approximately 154.3 ± 1.3 nm with a polydispersity index (PDI) of 0.191 ± 0.006, which was largely similar to the trehalose-mixed LNP (TM-LNP) and the TL-LNP. The zeta potential of the TL-LNP was 25.9 ± 0.6 mV, while TM-LNP and TL-LNP exhibited slightly higher values, around 28 mV (Fig. 2B). The trehalose encapsulation

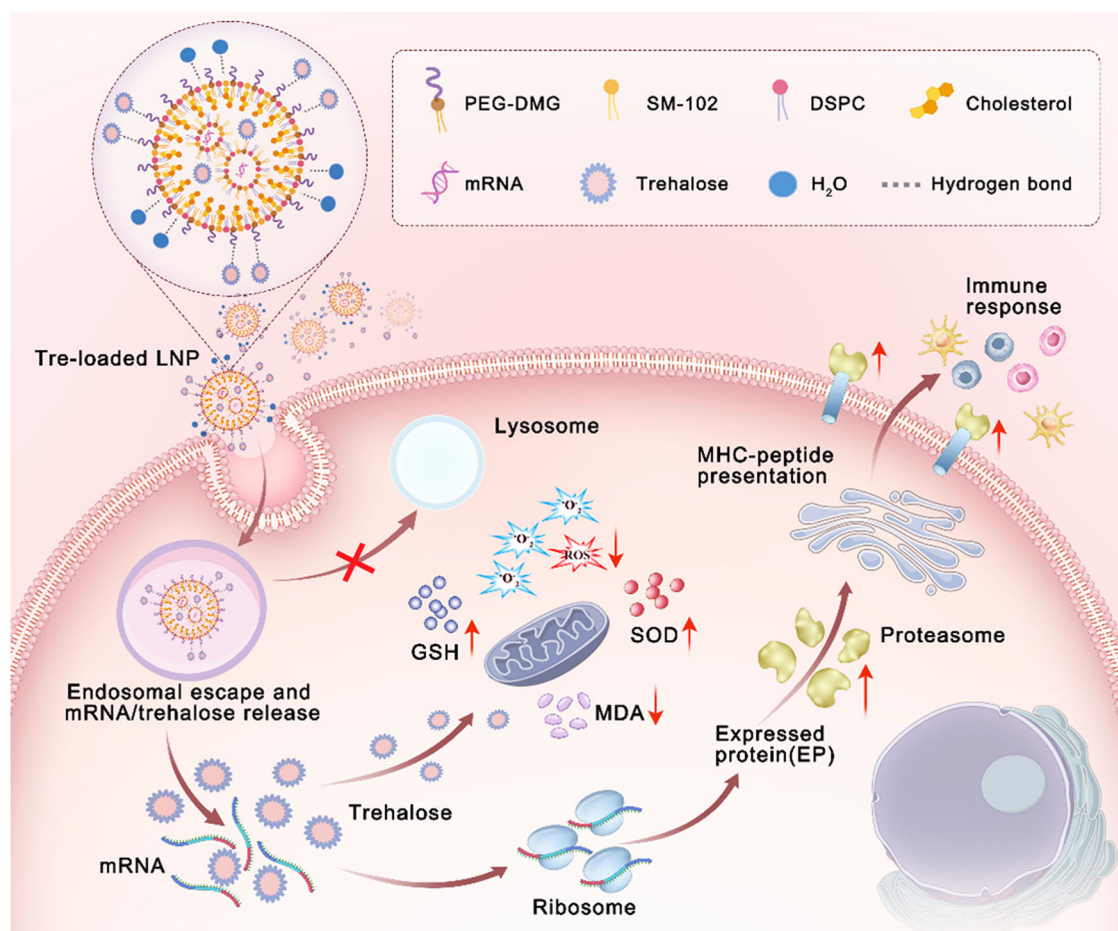
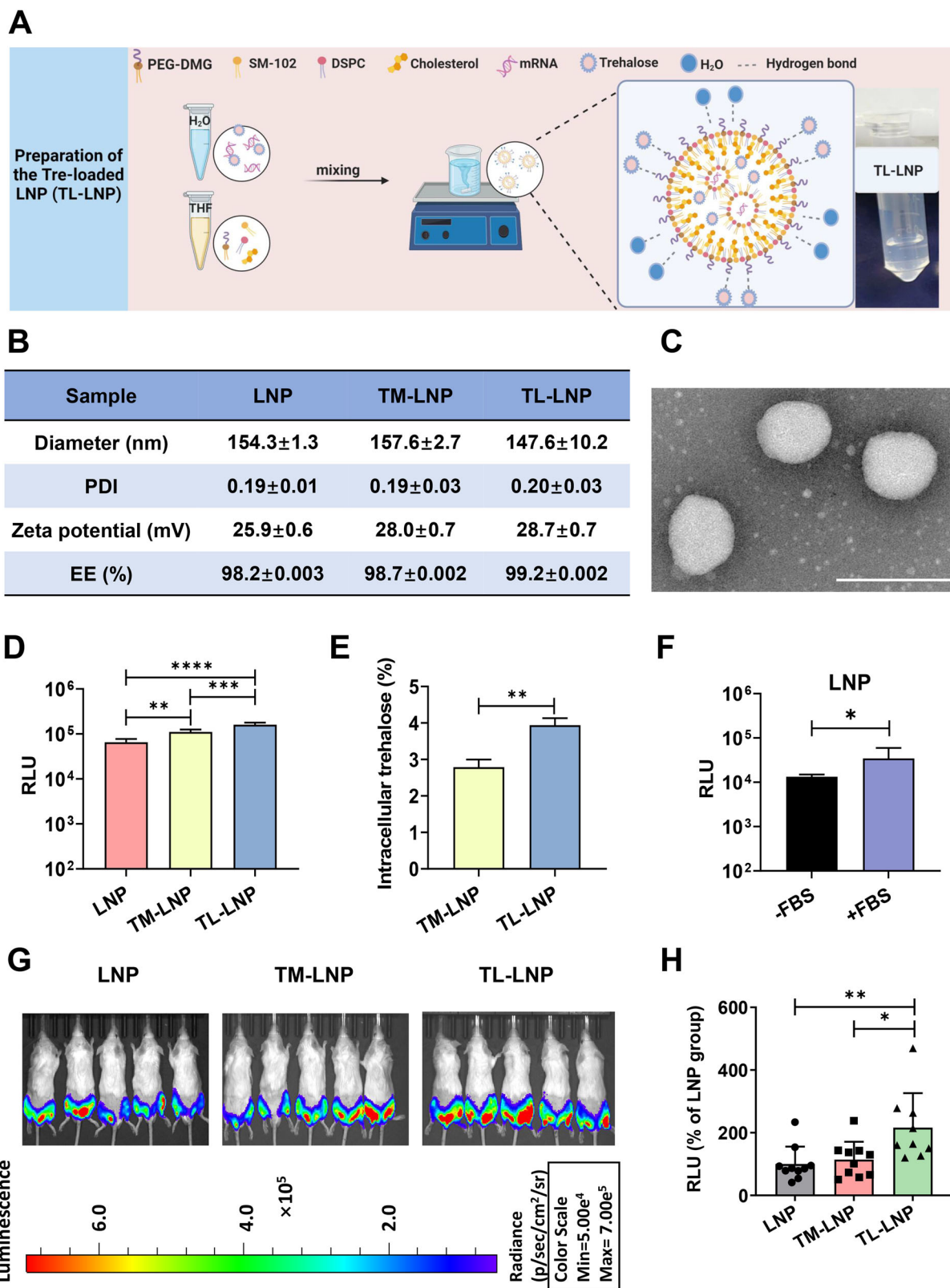


Fig. 1 | Schematic graph of the intracellular transport of Tre-loaded LNP (TL-LNP) and mechanism of enhanced mRNA transfection through decreased oxidative stress by trehalose. Following endocytosis-mediated internalization into lysosomes, TL-LNP achieves cytoplasmic entry via lysosomal escape, concomitant with

co-release of mRNA payload and trehalose. The released trehalose mitigates nanoparticle-induced oxidative stress through free radical scavenging, thereby reducing LNP-associated cytotoxicity and enhancing target protein expression efficiency.



efficiency for TL-LNP was $17.7 \pm 0.9\%$. TEM graph in Fig. 2C showed the morphology of LNP, which was consistent with the DLS results. Control formulations were additionally prepared in PBS buffer (pH 7.4) for comparative analysis. Lipid nanoparticles (LNPs), trehalose-mixed LNPs (TM-LNPs), and trehalose-loaded LNPs (TL-LNPs) were formulated and characterized (Supplementary Table 1). The data demonstrate that PBS-

prepared LNPs exhibit acceptable colloidal stability for biological applications: diameter 179.5 nm (PDI \approx 0.14, near-neutral zeta potential), while TM-LNPs and TL-LNPs showed larger sizes (248.9 nm and 222.2 nm, respectively)—both within acceptable ranges for in vivo delivery (<250 nm, PDI < 0.3). LNPs prepared in RNase-free water instead of PBS exhibit significantly reduced size variation and enhanced stability during trehalose

Fig. 2 | Preparation and characterization of TM-LNP and TL-LNP: Evaluation of in vitro and in vivo transfection efficiency. **A** Schematic graph illustrating the preparation of TL-LNP. Created by BioRender.com. **B** Characterization including size distribution, zeta potential, PDI and mRNA encapsulation efficiency of freshly prepared LNP, TM-LNP and TL-LNP. **C** The TEM graph of LNP formulation. Bar = 200 nm. **D** The transfection efficiency of freshly prepared LNP, TM-LNP and TL-LNP on HEK293T cells at $0.5 \mu\text{g mL}^{-1}$ of mRNA for 24 h ($n = 5$). Statistical analysis was performed using ordinary one-way ANOVA, $**p < 0.01$, $***p < 0.001$, $****p < 0.0001$. **E** After treatment with TM-LNP or TL-LNP at $0.5 \mu\text{g mL}^{-1}$ of mRNA for 8 h, the percentage of trehalose in HEK293T cells relative to the amount

of trehalose contained in the formulation added ($n = 3$). Statistical analysis was performed using *t*-test, $**p < 0.01$. **F** The transfection efficiency of freshly prepared mRNA-loaded LNP without trehalose on HEK 293 cells at $0.5 \mu\text{g mL}^{-1}$ of mRNA for 24 h in the absence or presence of FBS ($n = 5$). Statistical analysis was performed using *t*-test, $*p < 0.05$. **G** Visualization of *l*Luc bioluminescence and **H** quantification of *l*Luc expression in Balb/C male mice after intramuscular (IM) injection in both hind leg quadriceps muscles with freshly prepared LNP, TM-LNP, or TL-LNP, respectively ($n = 10$). Statistical analysis was performed using ordinary one-way ANOVA, $*p < 0.05$, $**p < 0.01$.

mixing or loading, primarily by mitigating salt-induced aggregation and precipitation. Even under in vivo physiological conditions (pH 7.4), their hydrodynamic properties conform to functional specifications, ensuring uncompromised biological functionality. The observed reduction in encapsulation efficiency across all three PBS-formulated LNP groups arises from synergistic ionic-trehalose interference—specifically, PBS-derived salt ions compromising lipid-nucleic acid complexation through charge screening. Critically, PBS-formulated LNPs fail to fully replicate the physiological behavior of their RNase-free water counterparts in in vivo environments, particularly given the limited exposure to systemic fluids in intramuscular administration. These findings unequivocally validate the strategic superiority of RNase-free water-phase preparation for preserving mRNA vaccine integrity and delivery efficacy. Then the in vitro transfection efficiency of these formulations was evaluated on HEK293T cells. Figure 2D showed that LNPs with trehalose (TM-LNP and TL-LNP) significantly improved transfection efficiency compared to those without trehalose, with TL-LNP outperforming both TM-LNP ($***p < 0.001$) and LNP without trehalose ($****p < 0.0001$). This observation suggests that the incorporation of trehalose plays a crucial role in modulating transfection efficiency by altering cell state, as the characteristics (e.g., size distribution, zeta potential, and PDI) of LNP, TM-LNP, and TL-LNP were nearly identical. Given the physicochemical properties of these LNPs showed minimal changes, we anticipate negligible variations in cellular uptake of these groups. This indicates that the major cause of the substantial variances in transfection efficiency presumably resides in intracellular processes. Since trehalose is present in both the TM-LNP and TL-LNP formulations, it is inevitable that a part of it will be internalized by transfected cells during in vitro transfection. Given that trehalose is a membrane-impermeable molecule^{21,22}, the transport of trehalose from the extracellular to the intracellular environment will definitely be different between the TM-LNP and TL-LNP groups, despite the overall concentration of trehalose in the cell culture medium during transfection is identical for both. Figure 2E showed that the TL-LNP could transport more trehalose in cells during transfection compared to the TM-LNP ($**p < 0.01$). Studies have shown that trehalose enhances transgene expression when coexisting with DNA-PEI complexes during transfection¹⁶. Leveraging its known ability to alleviate oxidative stress and protect cells from damage caused by oxygen radicals^{19,23–26}, trehalose may improve transfection efficiency by reducing the cytotoxicity of cationic LNPs and enhancing cell viability. This result implied that cell status plays a crucial role in transfection efficacy. To further substantiate our findings, we examined the influence of serum on transfection efficiency and found a significant difference in transfection efficiency with or without serum ($*p < 0.05$) in Fig. 2F. This may be attributed to the presence of abundant compounds in serum, including growth factors, vitamins, and amino acids, which promote cell viability and enhance transfection efficiency. This underscores the importance of cell state in transfection and supports our hypothesis that trehalose enhances transfection efficiency by optimizing the intracellular environment. Finally, the in vivo transfection efficiency of the freshly prepared LNP, TM-LNP and TL-LNP was evaluated. Figure 2G, H demonstrated that the expression of luciferase in the TL-LNP group was significantly higher than that in both the LNP ($**p < 0.01$) and TM-LNP ($*p < 0.05$) groups, which was consistent with the in vitro results. As another prevalent lyoprotectant in industrial applications, sucrose was systematically evaluated in parallel control experiments to benchmark the

performance of our trehalose-based strategy. While sucrose-mixed LNP (SM-LNP) exhibited superior in vitro transfection efficiency compared to conventional LNP, its in vivo performance aligned closely with standard LNP bioluminescence levels. Strikingly, sucrose-loaded LNP (SL-LNP) showed markedly reduced signals in both experimental settings (Supplementary Figs. 1, 2). The substitution of lyoprotectant from trehalose to sucrose necessitated formulation optimization, particularly for SL-LNP. The current sucrose concentration may represent a suboptimal parameter, potentially compromising the colloidal stability of LNPs through altered ionic interactions within the formulation matrix (Supplementary Table 2). These findings collectively suggest that sucrose modification does not enhance transfection efficiency under the implemented experimental conditions.

After validating the enhanced transfection efficiency mediated by trehalose in liquid formulation, we further examined the effect of trehalose present as a cryoprotectant on freeze-dried formulations. Two major challenges exist for the stability of the mRNA formulation post freeze-drying: the colloidal stability of the LNP as the mRNA delivery system and the chemical stability of the mRNA itself. The colloidal stability of the LNP can be easily damaged by the formed ice crystal during the freezing phase²⁷. Meanwhile, the vacuum environment during the drying phase would also cause the collapse of LNP and difficulties in reconstitution^{9,28}. Furthermore, the chemical integrity of mRNA itself could also be damaged during the freeze-drying. Both the colloidal stability of the LNP and the chemical stability of the mRNA itself were assessed as they could significantly compromise the overall stability of the mRNA formulations during the “pre-freezing” and “drying” phases (Fig. 3A).

The concentration of cryoprotectants and the pre-freezing temperature were the key parameters that needed optimization. Based on concentrations commonly reported in the literature, 20% (w/v) trehalose was selected^{10,29}. Additionally, the freezing temperatures of -20°C and -80°C were studied. It was observed that the rehydrated formulations pre-frozen at -80°C exhibited significantly smaller particle sizes and lower PDI compared to those frozen at -20°C (Fig. 3B–D). This was attributed to the lower temperature and rapid freezing rate, which reduced the formation of large ice crystals and minimized their disruptive effect on the size distribution of the LNP^{10,30,31}. Therefore, -80°C was selected as the pre-freeze temperature. In addition to the size distribution, zeta potential, and PDI, the mRNA encapsulation efficiency of both TM-LNP and TL-LNP was also well maintained after freeze-drying (Fig. 3E). These results indicated that the colloidal stability of the LNP was effectively preserved. After reconstitution, the FD-LNPs without trehalose exhibited a diameter of approximately $699.6 \pm 61.8 \text{ nm}$, a PDI of 0.341 (>0.3 , indicating instability and non-uniformity), and a zeta potential of about $10.9 \pm 0.9 \text{ mV}$. This average size was much larger than their pre-lyophilization size ($\sim 154.3 \pm 1.3 \text{ nm}$, PDI = 0.19). The size distribution of rehydrated trehalose-free FD-LNPs is shown in Supplementary Fig. 3. These data further demonstrate the cryoprotective function of trehalose for the colloidal stability of LNP. Furthermore, the chemical stability (integrity) of mRNA itself was also assessed. After 24 h of freeze-drying, the FDTM-LNP and FDTL-LNP were promptly reconstituted, and the loaded mRNA was extracted for integrity analysis by gel electrophoresis. The pure mRNA and freshly prepared liquid LNP without trehalose were used as control. Figure 3F showed that the integrity of the mRNA in both FDTM-LNP and FDTL-LNP formulations remained largely

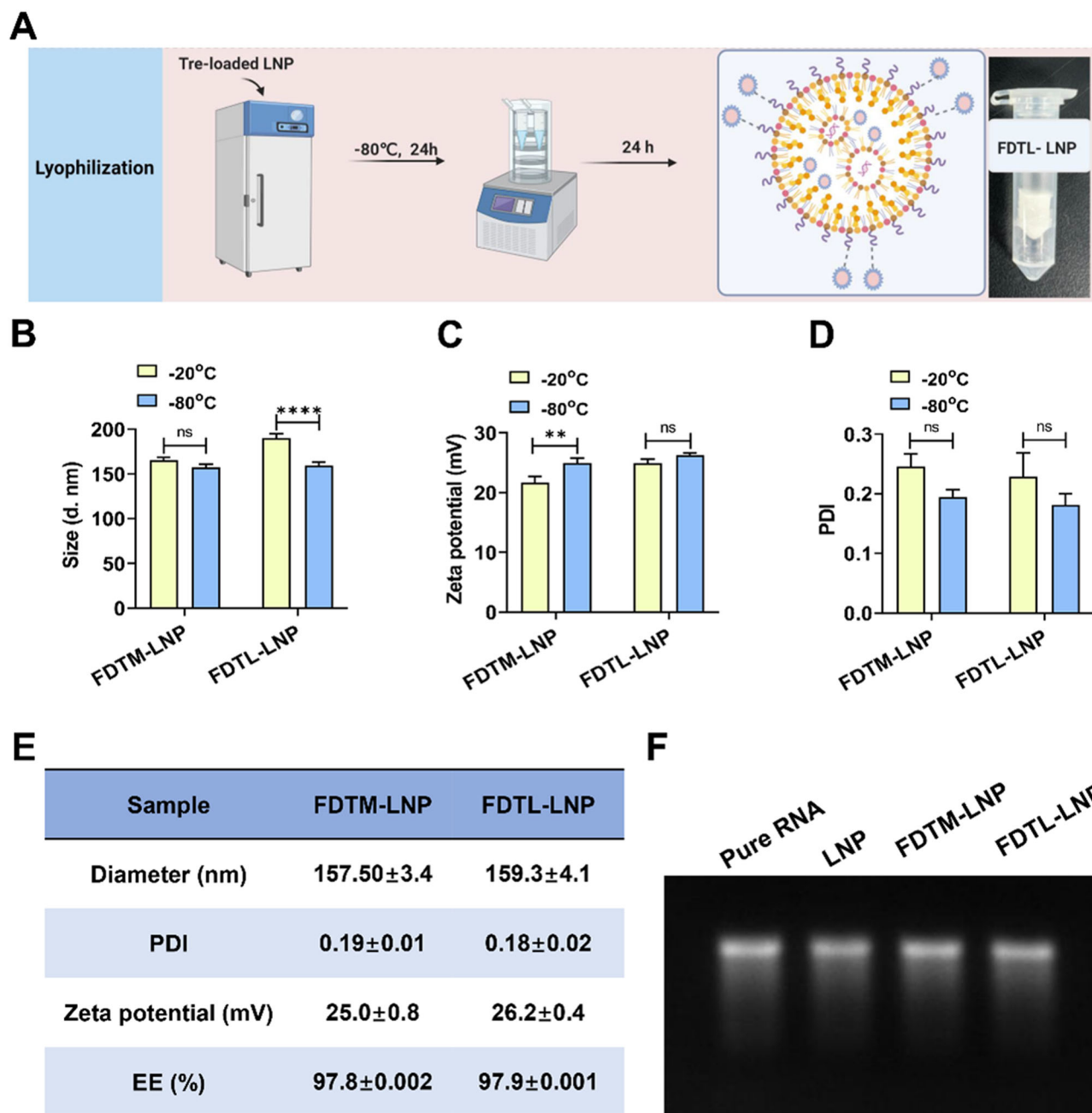


Fig. 3 | Preparation and characterization of freeze-dried trehalose-incorporated LNPs. **A** Schematic illustration of the preparation of freeze-dried trehalose-loaded LNP (FDTL-LNP). Created by BioRender.com. **B** The size distribution, **C** zeta potential and **D** PDI of FDTM-LNP and FDTL-LNP after pre-freezing at -80°C or -20°C for 24 h, freeze-drying for 24 h, and immediate reconstitution ($n = 3$). Statistical analysis was performed using Two-way ANOVA,

** $p < 0.01$, **** $p < 0.0001$. **E** Characterization of FDTM-LNP and FDTL-LNP after pre-freezing at -80°C for 24 h, freeze-drying for 24 h, and immediate reconstitution. **F** Gel bands of mRNA extracted from FDTM-LNP and FDTL-LNP samples following pre-freezing at -80°C for 24 h, freeze-drying for 24 h, and immediate reconstitution. Pure mRNA and freshly prepared LNP were used as control groups.

intact after freeze-drying. These findings provide a strong foundation for further exploration of their long-term storage stability, as the structural integrity of these formulations post-freeze-drying is a prerequisite for ensuring efficacy.

After storage at 4°C for various periods of time, samples were rehydrated and tested for in vitro transfection (Fig. 4A–D). Figure 4A showed that the transfection efficiency of FDTL-LNP after immediately reconstitution (week 0) was significantly higher than that of freshly prepared LNP (** $p < 0.001$). This result aligned with the transfection efficiency of the liquid formulations in Fig. 2D and confirmed the preserved colloidal and chemical stability of the formulations post-freeze-drying, as shown in Fig.

3E, F. Notably, the FDTL-LNP exhibited significantly higher in vitro transfection efficiency than the freshly prepared LNP without trehalose or the FDTM-LNP throughout the 4-week storage period at 4°C (Fig. 4B–D, Supplementary Fig. 4). Additionally, the FDTM-LNP showed comparable transfection efficiency compared to the freshly prepared LNP after 4 weeks (Fig. 4D), while its mRNA integrity retained only about 74% of the fresh mRNA (Fig. 4F). In contrast, the FDTL-LNP retained over 90% of mRNA integrity (Fig. 4E, F), indicating the chemical stability of mRNA was better preserved in FDTL-LNP. Comparative assessment of mRNA integrity in FDTL-LNP and FDTM-LNP formulations at 1-week and 2-week post-storage intervals revealed consistent degradation trends aligned with 4-week

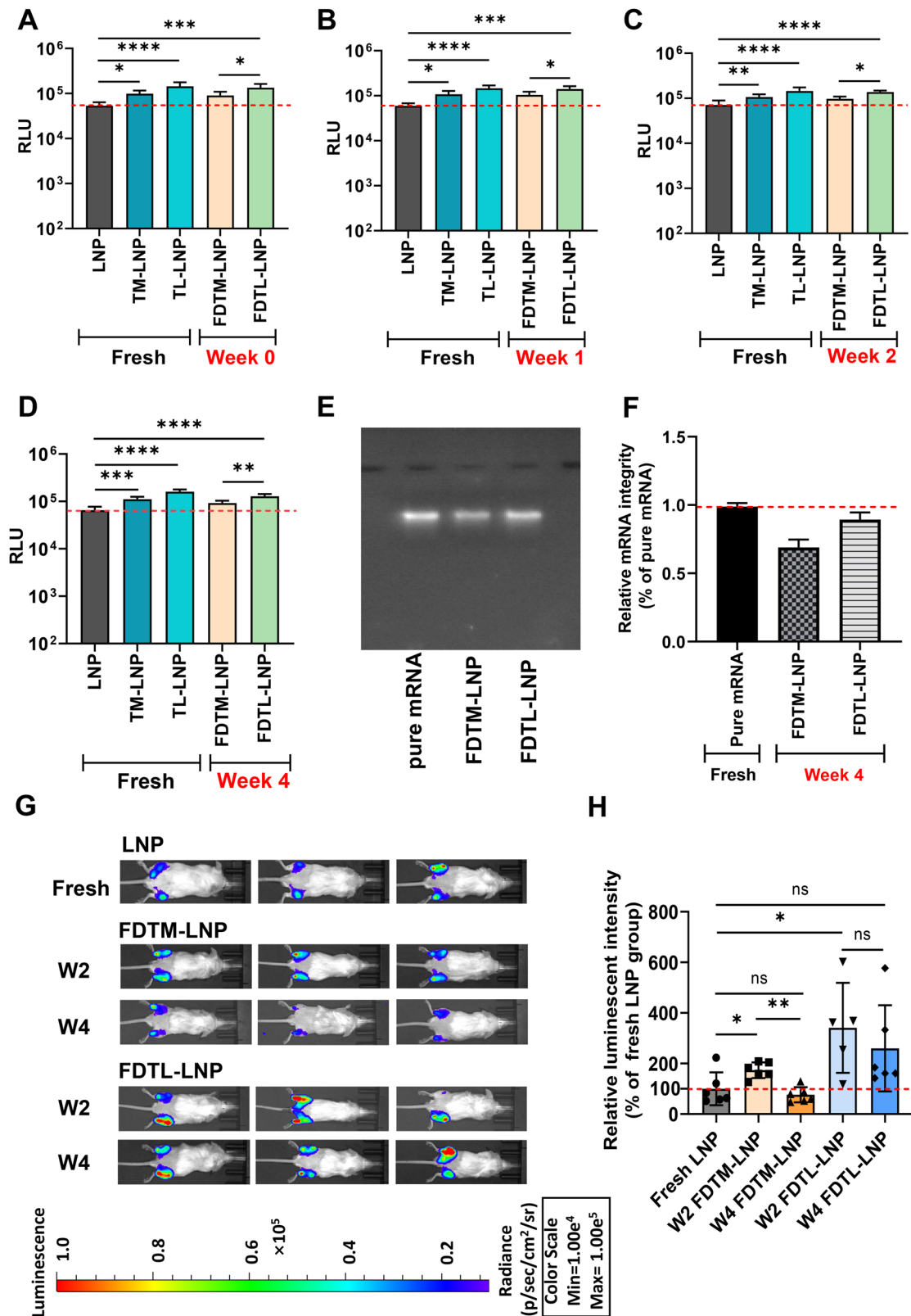


Fig. 4 | Transfection efficiencies and mRNA integrity of FDTM-LNP and FDTL-LNP after storage at 4 °C for various periods. A Transfection efficiencies of FDTM-LNP and FDTL-LNP after storage at 4 °C for 0 week, B 1 week, C 2 weeks and D 4 weeks on HEK293T cells, with freshly prepared LNP, TM-LNP, and TL-LNP as control groups ($n = 5$). Statistical analysis was performed using One-way ANOVA, $*p < 0.05$, $**p < 0.01$, $***p < 0.001$, $****p < 0.0001$. E The gel bands and F quantitative analysis of mRNA in FDTM-LNP and FDTL-LNP after storage at 4 °C

for 4 weeks analyzed using gel electrophoresis, with pure mRNA as control. G Visualization of fLuc bioluminescence and H quantification of fLuc expression in Balb/C male mice after intramuscular (IM) injection in both hind leg quadriceps muscles with TM-LNP or TL-LNP after storage at 4 °C for 2 or 4 weeks, respectively. Freshly prepared liquid LNP formulation was used as control ($n = 6$). Statistical analysis was performed using One-way ANOVA, $*p < 0.05$, $**p < 0.01$.

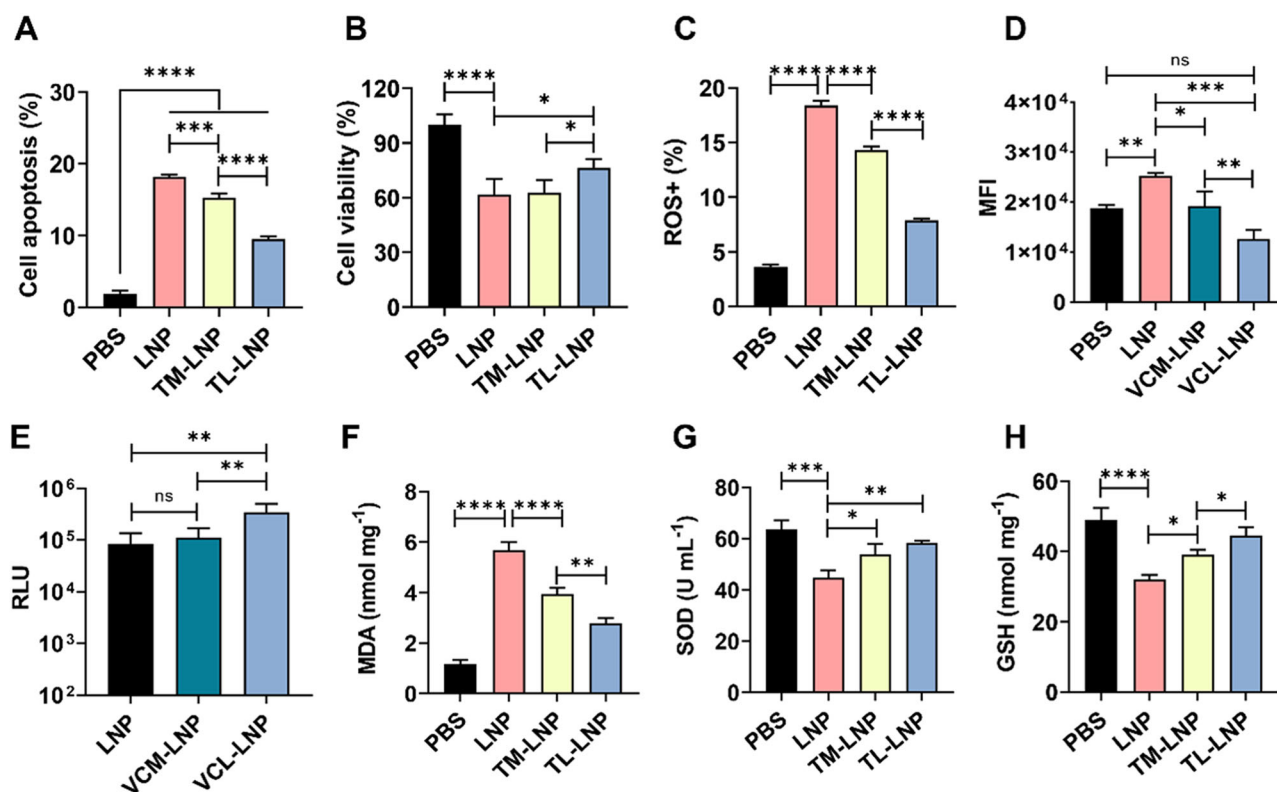


Fig. 5 | Differential modulation of intracellular redox homeostasis by various formulations. **A** Quantitative assessment of apoptosis in HEK293T cells after 4 h of incubation with different formulations at 0.5 $\mu\text{g mL}^{-1}$ of mRNA in FBS-free medium and an additional 24 h of culture in complete medium ($n = 3$). **B** Cell viability of HEK293T cells after 8 h of incubation with different formulations at 0.5 $\mu\text{g mL}^{-1}$ of mRNA in FBS-free medium and an additional 24 h of culture in complete medium ($n = 5$). **C** Percentage of intracellular ROS-positive cells after treatment with various formulations at 0.5 $\mu\text{g mL}^{-1}$ of mRNA for 4 h ($n = 3$). **D** Intracellular mean

fluorescence intensity of DCF after incubation with various formulations for 4 h ($n = 3$). **E** Transfection efficiency of HEK293T cells after treatment with LNP, VCM-LNP and VCL-LNP at 0.5 $\mu\text{g mL}^{-1}$ of mRNA ($n = 5$). **F** The intracellular concentration of MDA, **(G)** SOD and **(H)** GSH in HEK 293 T cells after treatment with various formulations at 0.5 $\mu\text{g mL}^{-1}$ of mRNA for 8 h ($n = 3$). Statistical analysis was performed using One-way ANOVA, * $p < 0.05$, ** $p < 0.01$, *** $p < 0.001$, **** $p < 0.0001$.

observations, with FDTL-LNP demonstrating significantly superior preservation capacity across all timepoints (Supplementary Fig. 5). These results suggested that the internal trehalose loaded within the LNP plays a crucial role in preserving mRNA chemical stability. This is likely achieved through a “hydrogen bond replacement” mechanism, where trehalose form hydrogen bonds with mRNA, replacing those between water and mRNA during lyophilization to maintain its native conformation and stability.

The *in vivo* bioluminescence imaging of the FDTM-LNP and FDTL-LNP was then analyzed. After being stored at 4 °C for 2 weeks, both the FDTM-LNP and FDTL-LNP groups demonstrated *in vivo* luminescent intensity approximately 173% and 341% of those observed with the freshly prepared LNP. Even after 4 weeks, the FDTL-LNP showed a negligible decrease. However, the FDTM-LNP after 4 weeks showed obviously decreased protein expression compared to those stored for 2 weeks (** $p < 0.01$), retaining only about 76% of the luminescent intensity of the fresh LNP group (Fig. 4G–H), although its *in vitro* performance remained higher than that of the fresh LNP (Fig. 4D). This phenomenon has also been reported in literatures^{8,10,12}. We speculate that this discrepancy likely arises from the biological effects of trehalose on transfected cells, influenced by the inherent differences between *in vivo* and *in vitro* environments. The diminished *in vivo* performance of FDTM-LNP may result from the rapid diffusion of external trehalose, which interferes with its co-delivery with LNPs into targeted antigen-presenting cells (APCs). Although the FDTM-LNP exhibited good *in vitro* performance, it was attributed to the effect of trehalose on cell protection rather than the inherent stability of mRNA itself. Once trehalose fails to be co-delivered into cells, the *in vivo* efficacy of FDTM-LNP may obviously decline after long-term storage. This issue is

particularly concerning as this may lead to inaccurate vaccine efficacy assessments and pose a risk of using ineffective vaccines. In contrast, our approach offers a significant advantage by ensuring better preservation and sustained *in vivo* efficacy during long-term storage.

However, the lyophilized sucrose-modified LNPs detailed in Supplementary Fig. 6 showed more pronounced signal attenuation following storage. Notably, the SL-LNP formulation displayed increased hydrodynamic diameter following lyophilization ($\sim 325.9 \pm 18.6$ nm, Supplementary Table 2), which may be attributed to suboptimal sucrose concentration parameters in the loading protocol. This non-optimized formulation condition potentially compromises colloidal stability through altered ionic interactions and freeze-drying, consequently diminishing *in vivo* transfection efficacy. Collectively, these results demonstrate that sucrose-based modification fails to enhance transfection efficiency under current experimental parameters, while highlighting the critical need for formulation optimization when substituting lyoprotectants.

As it’s challenging to detect intracellular trehalose in target cells *in vivo*, we utilized an *in vitro* model to analyze intracellular trehalose content, redox levels, and the corresponding transfection efficiencies to validate our hypothesis. Previous results in Fig. 2E have proved that the intracellular trehalose of TL-LNP was significantly higher than the TM-LNP (** $p < 0.01$). It is well established that cationic LNPs can compromise cell membrane integrity, induce oxidative stress, and exert detrimental effects on mitochondria and lysosomes, ultimately reducing cell viability³². Given the critical role of trehalose in cellular protection^{33,34}, we further compared the cell viability, intracellular redox level, and transfection efficiency of HEK293T cells after incubation with various formulations. The results

indicated that TL-LNP significantly reduced cell apoptosis (Fig. 5A and Supplementary Fig. 7) and markedly improved cell viability compared to TM-LNP (Fig. 5B). Previous studies have reported that trehalose plays a direct role in scavenging ROS (e.g., H_2O_2 and O_2^-)¹⁸. Our results in Fig. 5C showed that the percentage of ROS-positive cells increased significantly after incubation with LNPs for 4 h ($****p < 0.0001$), while formulations containing trehalose, especially TL-LNP, significantly decreased the proportion of ROS-positive cells. To assess whether the oxidative stress influences transfection efficiency, the well-known antioxidant Vitamin C (VC) was used as a positive control. Supplementary Fig. 8 shows the intracellular 2',7'-Dichlorofluorescein (DCF) fluorescence graph of HEK293 cells after incubation with various formulations. Figure 5D, E presented that the VC-loaded LNP (VCL-LNP) effectively reduced intracellular ROS levels, and significantly enhanced LNP-mediated transfection efficiency, with VCL-LNP outperforming VC-mixed LNP (VCM-LNP). Key intracellular indicators and enzymes related to redox balance were also analyzed. Intracellular malondialdehyde (MDA) often results from the excessive generation of reactive oxygen species or insufficient antioxidant defense mechanisms. The elevated intracellular MDA content in the LNP group indicated that cells had experienced oxidative stress and lipid peroxidation. In contrast, groups with trehalose involvement significantly reduced MDA levels, with the TL-LNP group showing a more pronounced reduction compared to the TM-LNP group ($**p < 0.01$) in Fig. 5F. Intracellular superoxide dismutase (SOD) is an important antioxidant enzyme that evaluates cellular oxidative stress levels by catalyzing reactions to reduce intracellular superoxide radicals, which is crucial for maintaining cellular redox equilibrium. An obviously reduction in intracellular SOD level was observed after treatment with the LNP in Fig. 5G ($***p < 0.001$), while both the TM-LNP and TL-LNP groups demonstrated a notable increase in intracellular SOD compared to the LNP group ($*p < 0.05$ and $**p < 0.01$, respectively). Glutathione (GSH) is capable of neutralizing oxygen-free radicals, harmful metabolic byproducts, and various oxidative stress inducers. In Fig. 5H, the LNP group showed decreased GSH levels compared to normal cells ($****p < 0.0001$), while both TM-LNP and TL-LNP groups displayed increased intracellular GSH content than the LNP group. Additionally, the TL-LNP group had a notably higher GSH concentration than the TM-LNP group ($*p < 0.05$). An elevated intracellular GSH typically signifies a reinforced antioxidative defense within the cells, enabling them to combat oxidative stress and ameliorate oxidative damage. To sum up, the TL-LNP significantly reduced the cytotoxicity of the formulation and enhanced the transfection efficiency by decreasing the intracellular oxidative stress.

Nuclear factor erythroid 2-related factor 2 (Nrf2) is a crucial transcription factor that migrates to the nucleus, where it binds to the antioxidant response element (ARE)^{18,26}. This interaction triggers the transcription of target genes, thereby promoting detoxification and reducing oxidative stress. As an important effector in regulating intracellular oxidative stress, it can serve as an intracellular oxidative stress indicator. Cationic LNPs are well known to induce oxidative stress. Figure 6A demonstrated that intracellular Nrf2 expression was significantly elevated and predominantly localized in the nucleus following incubation with the LNP, correlating with increased oxidative stress. However, after treatment with TM-LNP or TL-LNP, Nrf2 expression in both the nucleus and cytoplasm was markedly reduced (Fig. 6B), showing trehalose lowers oxidative stress and Nrf2 activation. Although trehalose has been reported to enhance Nrf2 expression for protection against oxidative stress²⁶, our results do not contradict these findings. Nrf2 activation can be influenced by various factors, with levels fluctuating based on the timing of measurement, particularly as cells adapt to oxidative stress. In the early stages of oxidative stress, Nrf2 activation rises sharply as part of the cellular defense mechanism to counteract oxidative damage. However, as oxidative stress subsides, Nrf2 expression may decrease, reflecting a reduced need for its protective role^{35–37}. For example, Lin Wang et al. found that trehalose treatment significantly inhibited Cd-stimulated nuclear translocation of Nrf2 and the subsequent elevated expression of Nrf2-downstream targets in rat liver³⁶. In our study, the effect of LNPs resembled that of Cd as described in the literature above. The addition of trehalose to the LNPs

significantly reduced intracellular oxidative stress, leading to a marked suppression of Nrf2 expression and its nuclear translocation, indicating a reduced cellular need for Nrf2's protective function.

Discussion

We have successfully developed a novel approach that markedly differs from conventional lyophilization methods, which often rely on complex protocols such as batch freeze-drying or continuous spin lyophilization and typically entail simply blending the formulation with trehalose. Importantly, our method does not require any additional excipients beyond standard lyoprotectants (trehalose), which are already ubiquitously employed in conventional workflows. In our innovative methodology, trehalose is not only situated externally to the LNP but is also co-encapsulated with mRNA within the formulation to mitigate mRNA degradation and LNP aggregation. Externally, trehalose enwraps the LNP within a solid, amorphous vitrified sugar matrix, thereby safeguarding its colloidal stability during a simplified 48-h freeze-drying process. Internally, trehalose forms hydrogen bonds with the encapsulated mRNA, impeding its mobilization and augmenting its chemical stability—achieving equivalent or superior long-term stability compared to conventional methods.

Moreover, the encapsulated trehalose is co-delivered with mRNA into target cells, substantially enhancing transfection efficiency by alleviating intracellular oxidative stress associated with the cationic LNP. This biological effect of trehalose co-delivery extends the effective storage duration under equivalent conditions, effectively enhancing the formulation's functional longevity and reducing the in vitro-in vivo efficacy gap. This cost-effective approach obviates the necessity for additional components, thereby diminishing potential immunological side effects.

By repurposing a single industry-standard excipient, our strategy directly addresses the limitations of conventional methods without introducing new components or costly process modifications. It also alleviates the exacting requirements for lyophilization procedures, as our method requires only a one-step process with optimized trehalose loading, further curtailing manufacturing costs and facilitating the transportation and distribution of mRNA-LNP formulations to remote regions, rendering it highly propitious for extensive adoption within the pharmaceutical industry.

Methods

Materials

Cationic lipid SM-102, 1,2-distearoyl-sn-glycero-3-PC (DSPC) and cholesterol were purchased from Rhawn (China). Polyethylene glycol dimyristoyl glycerol (PEG2000-DMG) was brought from Shanghai Macklin Biochemical Technology Co., Ltd. Tetrahydrofuran (THF), Bull serum albumin (BSA), Tween-20, and trehalose were purchased from Sigma-Aldrich. Trypsin-EDTA (0.25%, w/v), fetal bovine serum (FBS), and 1% penicillin/streptomycin were bought from Gibco (CA, USA). EZ Cap™ Firefly luciferase mRNA was purchased from Apexbio. Firefly Glo Luciferase Reporter Gene Assay Kit was obtained from Yeasen (Shanghai, China). Phosphate-buffered saline (PBS), DMEM medium were obtained from Hyclone Lab (UT, USA). RNase-free water and TPCK-trypsin were purchased from Thermo Fisher Scientific (UK). Trehalose Assay Kit was purchased from Nuominkeda (Wuhan, China) Biotechnology Co., Ltd. RiboGreen assay kit was purchased from Thermo Fisher. CCK8, malondialdehyde (MDA), superoxide dismutase (SOD), and glutathione (GSH) assay kits were purchased from Elabscience. RIPA buffer was purchased from Solarbio (Beijing, China). Reactive Oxygen Species (ROS) detection kit, Nuclear and Cytoplasmic Protein Extraction Kit, and Annexin V-FITC/PI apoptosis detection kit were obtained from Beyotime. Goat Anti-Rabbit IgG H&L polyclonal antibody FITC (PTB96441) and Anti-NFE2L2 polyclonal antibody were purchased from Antibody System (France).

Preparation and characterization of trehalose-loaded LNP (TL-LNP) in aqueous form

mRNA-loaded LNPs in aqueous form were synthesized using a one-step nanoprecipitation and solvent evaporation method. An organic phase was

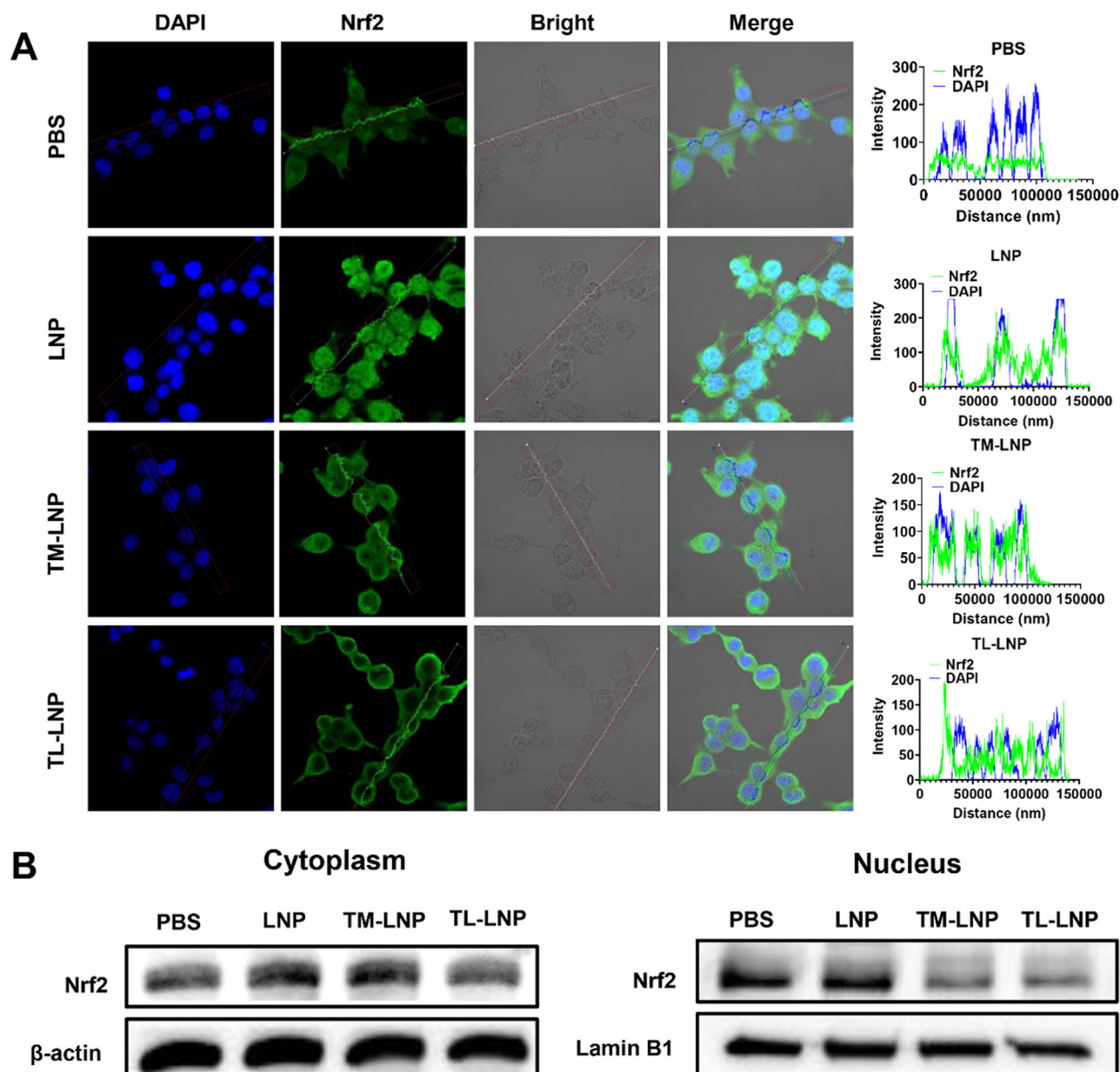


Fig. 6 | Intracellular Nrf2 signaling modulation after treatment with various formulations. **A** Visualization and localization of intracellular Nrf2 in HEK293T cells after treatment with freshly prepared LNP, TM-LNP, or TL-LNP for

8 h, including analysis of Nrf2 co-localization with the nucleus. **B** Western blotting analysis of Nrf2 in both the cytoplasm and nucleus of HEK293T cells following incubation with various formulations for 8 h.

prepared by dissolving SM-102, DSPC, cholesterol, and PEG2000-DMG in a molar ratio of 3.5:2.7:7:1 in THF/methanol (v/v = 6/1) mixed solvent. An aqueous phase of RNase-free water containing mRNA encoding luciferase was employed. The organic phase containing dissolved lipids is mixed with the aqueous phase containing mRNA at a volume ratio of 1:3, with an N/P ratio of SM-102 to mRNA is 6:1. The mixture is continuously stirred under a fume hood, allowing organic solvents to evaporate thoroughly, resulting in the formation of mRNA-loaded LNP formulation. For the trehalose-loaded LNP, abbreviated as TL-LNP, four lipids were dissolved in the THF/methanol mixed organic solvent according to above mentioned proportions and mixed with the mRNA aqueous solution, which contains 20% of trehalose (w/v). The trehalose-mixed LNP (abbreviated as TM-LNP) was prepared by directly adding trehalose to the obtained LNP suspension to achieve a final trehalose concentration of 20% (w/v), equivalent to 200 mg mL⁻¹. In parallel control experiments, sucrose-formulated LNPs were prepared using identical methodologies by substituting trehalose with

sucrose as the lyoprotectant: sucrose-mixed LNP (SM-LNP) through post-synthesis addition, and sucrose-loaded LNP (SL-LNP) via co-formulation with 20% sucrose (w/v) in the aqueous phase. All formulations were prepared using RNase-free water (pH 6.2 ± 0.2). The size distribution and zeta potential of all these samples were tested by DLS (Malvern, UK). Parallel formulations prepared in PBS (phosphate-buffered saline, pH = 7.4) served as controls to isolate buffer-specific effects. The morphology of the mRNA-loaded LNP without trehalose was observed by TEM. The encapsulation efficiency of mRNA was determined using the RiboGreen assay kit. Samples were diluted to an appropriate concentration with 1× TE buffer, mixed with the RiboGreen detection solution in equal proportions, and the fluorescence intensity was measured using a fluorescence spectrophotometer to calculate the concentration of free mRNA in the samples. Then, the samples were diluted with 2% Triton-TE buffer to disrupt the LNP structure and release all the mRNA. The samples were again mixed with the RiboGreen detection solution in equal proportions, and the fluorescence intensity was measured

to determine the total mRNA concentration. The encapsulation efficiency of the mRNA was calculated using the following formula: Encapsulation Efficiency (%) = $1 - (C_{\text{free}} / C_{\text{total}}) \times 100\%$.

The encapsulation efficiency of trehalose within TL-LNP was assessed utilizing an ultrafiltration centrifugation technique. Specifically, TL-LNP samples were subjected to centrifugation at 5000 rpm for 2 h using ultrafiltration centrifugal tubes with a molecular weight cutoff (MWCO) of 3000 to remove the free trehalose. Then the samples were treated with 2% Triton-TE buffer to release all the encapsulated trehalose. The encapsulated trehalose was subsequently quantified via a trehalose assay kit and the encapsulation efficiency of trehalose was calculated according to the following formula: Encapsulation Efficiency (%) = $(C_{\text{loaded}} / C_{\text{total}}) \times 100\%$.

Cell culture

Human embryonic kidney (HEK293T) cells were obtained from the Procell Life Science & Technology Co., Ltd (Wuhan, China). Cells were cultured in high-glucose DMEM medium (Gibco) supplemented with 10% fetal bovine serum (FBS, Gibco) and 1% (v/v) penicillin/streptomycin (Gibco) in a humidified atmosphere with 5% CO₂ at 37 °C.

In vitro transfection

For the luciferase assay, HEK293T cells were seeded in 96-well plate at 5×10^4 /well density 48 h before transfection to reach 60 ~ 80% confluence. Following the removal of growth medium, 190 μL of fresh serum-free DMEM medium or completed DMEM medium was added per well, and 10 μL of LNP containing 100 ng mRNA was added. After 4 h of incubation, the transfection medium was replaced with growth medium, which was supplemented with 10% FBS and 1% (v/v) penicillin/streptomycin. The luciferase activity in 50 μL medium from transfected cells was assayed with 50 μL luciferase substrate after 24 h using a GloMax[®] Microplate Reader (Promega), and its activity was expressed as relative light units (RLU). Similarly, the transfection efficiencies of various formulations modified with trehalose or sucrose were also evaluated.

Animals

9-12-week-old male BALB/c mice used for animal experiments were purchased from Guangdong Medical Laboratory Animal Center. The mice were maintained under specific pathogen-free conditions at the animal facility in Shen Zhen University Laboratory Animal Center. All animal experiments were performed in strict accordance with the Regulations for the Care and Use of Laboratory Animals and Guideline for Ethical Review of Animals.

In vivo bioluminescence imaging

Mice were placed into groups of $n = 5$ and housed in a fully acclimatized room with free access to food and water. Animals were given an adaption time of at least 7 days before experiments. Mice were injected intramuscularly (IM) in both hind leg quadriceps muscles with freshly prepared LNP, TM-LNP, TL-LNP, SM-LNP, and SL-LNP (5 μg of fLuc mRNA per leg). After 48 h, the mice were injected intraperitoneally with 100 μL of D-Luciferin substrate and allowed to rest for 15 min. Mice were anesthetized in the induction chamber with isoflurane at a flow rate of 3 L min⁻¹ using the XGI-8 gas anesthesia system. Once anesthesia was successfully achieved, the mice were transferred to the imaging chamber and imaged on an IVIS[®] Spectrum In Vivo Imaging System, with isoflurane administered at a flow rate of 1 L min⁻¹. A signal from each injection site was quantified using Molecular Imaging Software and expressed as RLU. At the end of the experiment, mice were euthanized by intraperitoneal injection of sodium pentobarbital at a dose of 300 mg kg⁻¹.

Preparation and characterization of freeze-dried mRNA-LNP formulations

Freshly prepared TM-LNP and TL-LNP, each containing 16.7 μg mL⁻¹ of mRNA, were stored at -80 °C or -20 °C for 24 h, followed by freeze-drying for an additional 24 h to obtain the freeze-dried samples, referred to as

FDTM-LNP and FDTL-LNP, respectively. LNP without trehalose was also freeze-dried to serve as the control group. The lyophilized samples were then rehydrated and subjected to DLS analysis to evaluate particle size and zeta potential. The morphology of rehydrated FDTL-LNP was further examined using TEM. The encapsulation efficiencies of mRNA in FDTM-LNP and FDTL-LNP were also tested using the same method as mentioned above. After freeze-drying for 24 h, the resulting FDTM-LNP and FDTL-LNP samples were immediately rehydrated with 2% Triton-TE buffer to disrupt the LNP structures and release all the mRNA. Samples were then incubated at 95 °C for 1 min. A 2% agarose gel was prepared with 1× TAE and ethidium bromide (0.5 μg mL⁻¹), and 200 ng of mRNA per well was loaded for electrophoresis at 80 V for 15 min. Then the gel was stained in EB solution (0.5 μg mL⁻¹) for 30 min, and the RNA integrity was visualized using a gel imaging system, with pure mRNA and freshly prepared LNP serving as control groups.

Stability of freeze-dried mRNA-LNP formulations at refrigerated temperature

The obtained FDTM-LNP and FDTL-LNP samples according to the protocol mentioned above were hermetically sealed and stored at 4 °C for varying durations like 0, 1, 2, 3, and 4 weeks. The in vitro transfection efficiencies of these samples were then conducted at predetermined time intervals, and the freshly prepared LNP, TM-LNP and TL-LNP were evaluated as controls. Meanwhile, the in vivo luciferase expression of the FDTM-LNP or the FDTL-LNP samples stored at 4 °C for 2 or 4 weeks was also analyzed. Freeze-dried sucrose-formulated LNPs (FDSM-LNP and FDSL-LNP) were evaluated in parallel. The integrity of mRNA in FDTM-LNP or FDTL-LNP samples after storage at 4 °C for 1, 2, or 4 weeks was finally examined using the gel electrophoresis method.

Intracellular trehalose analysis

3×10^6 HEK293T cells were seeded in a 6-well plate and cultured for 48 h. Subsequently, the Tre-mixed LNP and Tre-loaded LNP containing 0.5 μg mL⁻¹ of mRNA were added and incubated in a serum-free medium. After 8 h, cells were washed with PBS, lysed with RIPA buffer, and sonicated to release all intracellular trehalose. Subsequently, the absorbance of the cell homogeneity was measured at 510 nm using a UV spectrophotometer following the instructions provided in the kit protocol. The intracellular trehalose was calculated based on the following formula: The intracellular trehalose content (%) = $(\text{Intracellular trehalose} / \text{Total added trehalose}) \times 100\%$.

Apoptosis analysis

3×10^6 HEK293T cells were seeded in 6-well plate for 48 h. Cells were incubated with various samples, including LNP, TM-LNP, or TL-LNP, each containing 0.5 μg mL⁻¹ of mRNA in serum-free medium for 4 h. Following this, the medium was replaced with complete medium, and the cells were incubated for an additional 24 h. The cells were collected, stained with Annexin V and PI, and analyzed using a flow cytometer.

Cell viability

5×10^4 HEK293T cells were seeded in a 96-well plate. After 48 h, cells were treated with various formulations including LNP, TM-LNP, or TL-LNP at 0.5 μg mL⁻¹ of mRNA in serum-free medium for 8 h. Then the medium was replaced with complete culture medium, and cells were further incubated for 24 h. Subsequently, the cell viability of HEK293T cells was evaluated using CCK8 assay.

Intracellular reactive oxygen species (ROS) detection

3×10^6 HEK293T cells were seeded in 6-well plate for 48 h. Then the HEK293T cells were treated with LNP, TM-LNP or TL-LNP, respectively at an mRNA concentration of 0.5 μg mL⁻¹ in serum-free medium for 4 h. Then the cells were collected and resuspended in the ROS fluorescent probe DCFH-DA solution (10 μM) to a final cell concentration of 3×10^6 cells mL⁻¹. The cell suspension was incubated at 37 °C in a cell incubator for 10 min, with

gentle inversion every 3–5 min to ensure thorough contact between the probe and the cells. Subsequently, the cells were washed with PBS for three times and detected using a flow cytometer.

Intracellular oxidative stress evaluation

3×10^6 HEK293T cells were seeded in 6-well plate. After 48 h, the cells were treated with various formulations, including LNP, TM-LNP, or TL-LNP, each containing $0.5 \mu\text{g mL}^{-1}$ of mRNA in serum-free medium. After 8 h, cells were washed, digested, and collected in $500 \mu\text{L}$ of PBS and subsequently homogenized in an ultrasonic homogenizer. The homogenate was then centrifuged at $10,000\times g$ for 10 min at 4°C , and the supernatant was collected and kept on ice for further analysis. The malondialdehyde (MDA), superoxide dismutase (SOD), and glutathione (GSH) contents were assessed using respective assay kit.

In vitro transfection and intracellular ROS detection of Vitamin C-incorporated LNP

Trehalose was replaced with Vitamin C (VC) for the preparation of VC-mixed LNP and VC-loaded LNP, abbreviated as VCM-LNP. The LNP, VC-mixed LNP, and VC-loaded LNP were added to HEK293T cells at concentrations of $50 \mu\text{M}$ VC and $0.5 \mu\text{g mL}^{-1}$ mRNA for 4 h. After 24 h, the transfection efficiency was analyzed.

5×10^4 HEK293T cells were seeded in a 96-well plate for 48 h. Similarly, the LNP, VC-mixed LNP, and VC-loaded LNP were added to HEK293T cells at concentrations of $50 \mu\text{M}$ VC and $0.5 \mu\text{g mL}^{-1}$ mRNA for 4 h. Then the cells were stained with DCFH-DA for 5 min and imaged by Microplate Reader (BioTek). The intracellular mean fluorescence intensity (MFI) in each group was analyzed by Gen5.

Intracellular location of Nrf2 associated with toxic and oxidative stress

2×10^5 HEK293T cells were seeded in a confocal dish for 48 h. After treatment with LNP, TM-LNP, or TL-LNP at $0.5 \mu\text{g mL}^{-1}$ of mRNA in serum-free medium for 12 h. Then the cells were fixed with 4% paraformaldehyde, permeabilized with 0.1% Triton X-100 in PBS for 15 min, and blocked with 2% BSA in PBS for 1 h at room temperature. The samples were then incubated overnight at 4°C with Anti-NFE2L2 polyclonal antibody. After PBS washing, the cells were incubated with Anti-Rabbit IgG H&L polyclonal antibody FITC for 1 h at room temperature, followed by PBS washing. Finally, all samples were stained with DAPI and observed under a confocal microscope.

Western blotting analysis of vaccine-associated changes in Nrf2

4×10^5 HEK293T cells were seeded in a 6-well plate for 48 h. Then cells were incubated with LNP, TM-LNP, or TL-LNP at $0.5 \mu\text{g mL}^{-1}$ of mRNA in serum-free medium for 12 h. Cells were washed with PBS, then the nuclei and cytoplasm were separated using Nuclear and Cytoplasmic Protein Extraction Kit. Proteins were denatured by heating at 90°C for 10–15 min. Samples were subjected to sodium dodecyl sulfate poly-acrylamide gel electrophoresis (SDS-PAGE) gels and transferred to polyvinylidene difluoride membranes. After blocking with 5% skimmed milk and washed with TBST, membranes were incubated with the primary antibodies and species-specific secondary antibodies. Finally, protein bands were detected by chemiluminescent analyzer using the ECL kit.

Data availability

No datasets requiring public deposition (e.g., sequencing, structural, or proteomics data) were generated in this study. All data generated or analyzed in this study are included in the published article and its supplementary information files. Source data can be made available upon request to the corresponding author.

Received: 4 December 2024; Accepted: 2 August 2025;
Published online: 20 August 2025

References

1. Stuart, L. M. In gratitude for mRNA vaccines. *N. Engl. J. Med.* **385**, 1436–1438 (2021).
2. Wang, Y. et al. mRNA vaccine: a potential therapeutic strategy. *Mol. Cancer* **20**, 33 (2021).
3. Blakney, A. K., Ip, S. & Geall, A. J. An update on self-amplifying mRNA vaccine development. *Vaccines* **9**, 97 (2021).
4. Pascolo, S. Synthetic messenger RNA-based vaccines: from scorn to hype. *Viruses* **13**, 270 (2021).
5. Uddin, M. N. & Roni, M. A. Challenges of storage and stability of mRNA-based COVID-19 vaccines. *Vaccines* **9**, 1033 (2021).
6. UN Environment Programme. Why optimized cold-chains could save a billion COVID vaccines, Why optimized cold-chains could save a billion COVID vaccines (unep.org), 2020 (accessed 26 June 2020)
7. Abdelwahed, W., Degobert, G., Stainmesse, S. & Fessi, H. Freeze-drying of nanoparticles: formulation, process and storage considerations. *Adv. Drug Deliv. Rev.* **58**, 1688–1713 (2006).
8. Muramatsu, H. et al. Lyophilization provides long-term stability for a lipid nanoparticle-formulated, nucleoside-modified mRNA vaccine. *Mol. Ther.* **30**, 1941–1951 (2022).
9. Li, M. et al. Lyophilization process optimization and molecular dynamics simulation of mRNA-LNPs for SARS-CoV-2 vaccine. *npj Vaccines* **8**, 153 (2023).
10. Zhao, P. et al. Long-term storage of lipid-like nanoparticles for mRNA delivery. *Bioact. Mater.* **5**, 358–363 (2020).
11. Meulewaeter, S. et al. Continuous freeze-drying of messenger RNA lipid nanoparticles enables storage at higher temperatures. *J. Controlled Release* **357**, 149–160 (2023).
12. Zhao, Y. et al. Optimization of heat-resistance technology for a duck hepatitis lyophilized live vaccine. *Vaccines* **10**, 269 (2022).
13. Sizovs, A. et al. Poly(trehalose): sugar-coated nanocomplexes promote stabilization and effective polyplex-mediated siRNA delivery. *J. Am. Chem. Soc.* **135**, 15417–15424 (2013).
14. Vinciguerra, D., Gelb, M. B. & Maynard, H. D. Synthesis and application of trehalose materials. *JACS Au* **2**, 1561–1587 (2022).
15. Bae, S. H. et al. A lipid nanoparticle platform incorporating trehalose glycolipid for exceptional mRNA vaccine safety. *Bioact. Mater.* **38**, 486–498 (2024).
16. Tseng, W. C., Tang, C. H., Fang, T. Y. & Su, L. Y. Trehalose enhances transgene expression mediated by DNA-PEI complexes. *Biotechnol. Prog.* **23**, 1297–1304 (2007).
17. Chen, S. et al. Comb-like pseudopeptides enable very rapid and efficient intracellular trehalose delivery for enhanced cryopreservation of erythrocytes. *ACS Appl. Mater. Interfaces* **12**, 28941–28951 (2020).
18. Benaroudj, N., Lee, D. H. & Goldberg, A. L. Trehalose accumulation during cellular stress protects cells and cellular proteins from damage by oxygen radicals. *J. Biol. Chem.* **276**, 24261–24267 (2001).
19. Pupyshev, A. B., Klyushnik, T. P., Akopyan, A. A., Singh, S. K. & Tikhonova, M. A. Disaccharide trehalose in experimental therapies for neurodegenerative disorders: Molecular targets and translational potential. *Pharmacol. Res.* **183**, 106373 (2022).
20. Kafetzis, K. N. et al. The effect of cryoprotectants and storage conditions on the transfection efficiency, stability, and safety of lipid-based nanoparticles for mRNA and DNA delivery. *Adv. Healthcare Mater.* **12**, e2203022 (2023).
21. Stewart, S. & He, X. Intracellular delivery of trehalose for cell banking. *Langmuir* **35**, 7414–7422 (2019).
22. Niu, Q. et al. Membrane stabilization versus perturbation by aromatic monoamine-modified gamma-PGA for cryopreservation of human RBCs with high intracellular trehalose. *J. Mater. Chem. B* **10**, 6038–6048 (2022).
23. Hu, Y. et al. Trehalose in biomedical cryopreservation-properties, mechanisms, delivery methods, applications, benefits, and problems. *ACS Biomater. Sci. Eng.* **9**, 1190–1204 (2023).

24. Eroglu, A. et al. Intracellular trehalose improves the survival of cryopreserved mammalian cells. *Nat. Biotechnol.* **18**, 163–167 (2000).
25. Zhang, X. G. et al. Effects of trehalose supplementation on cell viability and oxidative stress variables in frozen-thawed bovine calf testicular tissue. *Cryobiology* **70**, 246–252 (2015).
26. Mizunoe, Y. et al. Trehalose protects against oxidative stress by regulating the Keap1-Nrf2 and autophagy pathways. *Redox Biol.* **15**, 115–124 (2018).
27. Jakubek, Z. J., Chen, S., Zaifman, J., Tam, Y. Y. C. & Zou, S. Lipid nanoparticle and liposome reference materials: Assessment of size homogeneity and long-term -70 °C and 4 °C storage stability. *Langmuir* **39**, 2509–2519 (2023).
28. Shirane, D. et al. Development of an alcohol dilution-lyophilization method for the preparation of mRNA-LNPs with improved storage stability. *Pharmaceutics* **15**, 1819 (2023).
29. Athaydes Seabra Ferreira, H. et al. Cryoprotectant optimization for enhanced stability and transfection efficiency of pDNA-loaded ionizable lipid nanoparticles. *Int. J. Pharm.* **665**, 124696 (2024).
30. Yin, M. et al. Effect of temperature fluctuations during frozen storage on ice crystal distribution and quality of tilapia (*Oreochromis mossambicus*). *Food Chem.* **463**, 141104 (2024).
31. Ullah, J., Takhar, P. S. & Sablani, S. S. Effect of temperature fluctuations on ice-crystal growth in frozen potatoes during storage. *LWT-Food Sci. Technol.* **59**, 1186–1190 (2014).
32. Azamezhad, A., Samadian, H., Jaymand, M., Sobhani, M. & Ahmadi, A. Toxicological profile of lipid-based nanostructures: are they considered as completely safe nanocarriers?. *Crit. Rev. Toxicol.* **50**, 148–176 (2020).
33. Fuenteslopez, C. V. et al. Mesenchymal stem cell cryopreservation with cavitation-mediated trehalose treatment. *Commun. Eng.* **3**, 129 (2024).
34. Murray, A., Kilbride, P. & Gibson, M. I. Trehalose in cryopreservation. Applications, mechanisms and intracellular delivery opportunities. *RSC Med. Chem.* **15**, 2980–2995 (2024).
35. Qu, K. C., Wang, Z. Y., Tang, K. K., Zhu, Y. S. & Fan, R. F. Trehalose suppresses cadmium-activated Nrf2 signaling pathway to protect against spleen injury. *Ecotoxicol. Environ. Saf.* **181**, 224–230 (2019).
36. Gong, Z. G., Wang, X. Y., Wang, J. H., Fan, R. F. & Wang, L. Trehalose prevents cadmium-induced hepatotoxicity by blocking Nrf2 pathway, restoring autophagy and inhibiting apoptosis. *J. Inorg. Biochem.* **192**, 62–71 (2019).
37. Sun, L. et al. Trehalose targets Nrf2 signal to alleviate d-galactose induced aging and improve behavioral ability. *Biochem. Biophys. Res. Commun.* **521**, 113–119 (2020).

Acknowledgements

This research received financial support from Guangdong Basic and Applied Basic Research Foundation (2023A1515110428, 2025A1515012065), Shenzhen Medical Research Fund (D2401001), Shenzhen Science and Technology Program (JCYJ20240813142059020) and Shenzhen High-level Talent Scientific Research Start-up Foundation (827-000743).

Author contributions

Conceptualization was carried out by X.H. Liu. Data curation was performed by X.H. Liu and H.P. Song. Funding acquisition was handled by X.H. Liu. Investigation and project administration were conducted by X.H. Liu, H.P. Song, L.L. Tao, Z. Zhai, and J.X. Huang. Supervision was provided by Y.X. Cheng. The original draft was written by X.H. Liu. All authors have reviewed and approved this manuscript.

Competing interests

The authors declare no competing interests.

Ethics approval and consent to participate

All animal experiments were conducted in full compliance with the Regulations for the Care and Use of Laboratory Animals and the Guideline for Ethical Review of Animals (China, GB/T 35892-2018).

Additional information

Supplementary information The online version contains supplementary material available at <https://doi.org/10.1038/s41541-025-01253-3>.

Correspondence and requests for materials should be addressed to Yong-Xian Cheng.

Reprints and permissions information is available at <http://www.nature.com/reprints>

Publisher's note Springer Nature remains neutral with regard to jurisdictional claims in published maps and institutional affiliations.

Open Access This article is licensed under a Creative Commons Attribution-NonCommercial-NoDerivatives 4.0 International License, which permits any non-commercial use, sharing, distribution and reproduction in any medium or format, as long as you give appropriate credit to the original author(s) and the source, provide a link to the Creative Commons licence, and indicate if you modified the licensed material. You do not have permission under this licence to share adapted material derived from this article or parts of it. The images or other third party material in this article are included in the article's Creative Commons licence, unless indicated otherwise in a credit line to the material. If material is not included in the article's Creative Commons licence and your intended use is not permitted by statutory regulation or exceeds the permitted use, you will need to obtain permission directly from the copyright holder. To view a copy of this licence, visit <http://creativecommons.org/licenses/by-nc-nd/4.0/>.

© The Author(s) 2025